





Original Article

Gelatin sponge scaffolds loaded with adipose-derived mesenchymal stem cell secretome enhance full-thickness skin wound healing in rats

Amir Alesheikh ¹ , Tayyeb Ghadimi ^{2*} , Abbas Kazemi Ashtiani ³ , Abolfazl Abbaszadeh ⁴ 

¹ Plastic and Reconstructive Surgeon, Department of Plastic & Reconstructive Surgery, School of Medicine, Iran University of Medical Sciences, Tehran, Iran.

*Corresponding author and reprints: Tayyeb Ghadimi, Professor, Department of Plastic & Reconstructive Surgery, School of Medicine, Iran University of Medical Sciences, Tehran, Iran.

Email: ghadimi.t@iums.ac.ir

Received: 18 Dec 2025

Accepted: 29 Dec 2025

Published: 06 Jan 2026

Abstract

Background: Skin wounds that are full-thickness present a major clinical problem. Although cell-based treatments have limitations, the secretome of adipose-derived mesenchymal stem cells (ADMSCs) stimulates recovery through paracrine signaling. This study utilized a gelatin sponge scaffold as a biocompatible delivery platform for the ADMSC secretome, creating a cell-free therapeutic system.

Methods: Human ADMSCs were characterized. Their conditioned medium (secretome) was collected and analyzed for key growth factors. Gelatin sponge scaffolds were fabricated by freeze-drying and crosslinking, then loaded with the secretome. Scaffolds were characterized physico-chemically (SEM, FTIR, porosity, degradation). In vitro biocompatibility was tested on dermal fibroblasts. Gelatin/secretome scaffolds, gelatin-only scaffolds, or gauze were used to treat full-thickness excisional wounds in rats (n = 6 per group). Wound closure, histology, collagen, and angiogenesis were evaluated on days 10 and 20.

Results: ADMSCs expressed characteristic markers. The secretome contained hepatocyte growth factor (124.45 pg/mL), basic fibroblast growth factor-2 (42.18 pg/mL), and vascular endothelial growth factor (7.54 pg/mL). Scaffolds showed high porosity (85-90%) and supported high fibroblast viability/proliferation. In vivo, gelatin/secretome scaffolds achieved significantly faster wound closure (87.4 ± 4.3% on day 10; 98.7 ± 1.2% on day 20) versus controls (gelatin: 68.2 ± 5.7% and 92.1%; gauze: 62.5 ± 6.1%). They also promoted superior re-epithelialization, collagen deposition (62.4 ± 5.8%), and neovascularization (32.8 ± 4.6 vessels/field).

Conclusion: Gelatin scaffolds loaded with ADMSC secretome significantly enhance full-thickness wound healing by accelerating closure, improving tissue regeneration, and stimulating angiogenesis. This cell-free platform represents a promising strategy for clinical wound care.

Keywords: Adipose Tissue; Gelatin; Mesenchymal Stem Cells; Regenerative Medicine; Secretome; Tissue Engineering; Tissue Scaffolds; Wound Healing.

Cite this article as: Alesheikh A, Ghadimi T, Kazemi Ashtiani A, Abbaszadeh A. Gelatin sponge scaffolds loaded with adipose-derived mesenchymal stem cell secretome enhance full-thickness skin wound healing in rats. *Soc Determinants Health*. 2026;12(1):1-15. DOI: <http://dx.doi.org/10.22037/SDH.v12i1.51225>

Introduction

Full-thickness skin wounds, which extend through the epidermis and dermis into subcutaneous tissue,

represent a significant global clinical challenge with high morbidity and healthcare costs (1). The complex

physiological healing process is frequently impaired in conditions such as diabetes, vascular disease, and advanced age, leading to chronic, non-healing wounds (2-4).

Because of their immunomodulatory potential, multipotency, and strong paracrine production of bioactive substances, mesenchymal stem cells (MSCs) have become a key component of regenerative therapy (5, 6). Adipose-derived MSCs (ADMSCs) are particularly advantageous, given their abundant availability through minimally invasive harvest, high proliferative potential, and robust secretory profile (7, 8). Crucially, studies show that, rather than direct differentiation and engraftment at the wound site, ADMSCs' therapeutic benefits are mainly mediated by their paracrine effects (9,10).

The secretome, a complex mixture of growth factors (including bFGF, VEGF, IGF-1, EGF, TGF- β , and HGF), cytokines, chemokines, and extracellular vesicles, mediates this paracrine effect (11–14). By regulating inflammation, supporting angiogenesis, encouraging keratinocyte and fibroblast migration and proliferation, and aiding extracellular matrix remodeling, these elements coordinate wound healing (15, 16). Leveraging the secretome in a cell-free therapy offers substantial advantages over direct cell transplantation, including reduced regulatory complexity, eliminated risks related to cell viability and immunogenicity, and easier standardization, storage, and transport (17-20).

Gelatin, a denatured collagen, is a widely used biomaterial that meets these needs. It is highly biocompatible, biodegradable, non-immunogenic, and contains cell-adhesive RGD sequences (21-24). Processed via methods like freeze-drying, it can form three-dimensional scaffolds with tunable porosity and mechanical properties (25, 26). Chemical crosslinkers, such as EDC, can further enhance its structural stability and degradation profile (27, 28).

Integrating the ADMSC secretome into a gelatin scaffold creates a synergistic, cell-free platform: the scaffold provides critical structural support for cell infiltration and tissue integration, while the secretome delivers a sustained, multifaceted biochemical signal to drive healing (29, 30). Although previous studies have shown promise for MSC-derived products in wound healing, a comprehensive evaluation of gelatin/secretome composites for full-thickness wounds remains limited (31, 32).

This study aimed to develop and systematically evaluate gelatin sponge scaffolds loaded with human ADMSC secretome for the treatment of full-thickness skin wounds. The specific objectives were to isolate and characterize human ADMSCs, to quantify key growth factors in the conditioned medium (secretome), to fabricate and crosslink gelatin/secretome sponge scaffolds, to perform thorough physico-chemical characterization of the scaffolds, to assess in vitro biocompatibility using human dermal fibroblasts, and to assess the effectiveness of a treatment in vivo utilizing a rat model of full-thickness excisional wounds.

Methods

ADMSC Isolation and Culture

Human adipose tissue was collected from healthy donors having elective liposuction surgeries with institutional review board approval and informed consent. The tissue was processed within 4 hours of collection. The isolation protocol was as follows: The tissue was thoroughly washed in PBS (phosphate-buffered saline) containing 1% penicillin-streptomycin to eliminate blood cells and debris. The tissue was cleaned, then broken down into small pieces and digested for 45 minutes at 37°C with gentle stirring by 0.075% collagenase type I. A complete culture medium comprising the serum of 10% fetal bovine (FBS; Gibco, USA), 1% penicillin-streptomycin (Gibco, USA), and DMEM/F12 (Dulbecco's

Modified Eagle Medium/Nutrient Mixture F-12; Gibco, USA) was added to stop enzymatic digestion. The stromal vascular fraction (SVF) pellet was created by centrifuging the resultant cell suspension at $1200 \times g$ for ten minutes. The cells were plated into T-75 culture flasks after the pellet was resuspended in full media. The cultures were kept in a wet incubator with 5% CO₂ at 37°C. Every 3 days, the medium was changed. The cells were passaged using a 0.25% trypsin-EDTA solution once they achieved 80–90% confluence.

Flow Cytometry Analysis

The expression of mesenchymal and hematopoietic surface markers in ADMSCs at passage 3 was assessed using flow cytometry. The cells were gathered, washed with phosphate-buffered saline, and then incubated with fluorochrome-linked antibodies against CD105-PE, CD90-FITC, CD73-APC, CD34-PerCP, and CD45-APC-Cy7 for 30 minutes at 4°C in the dark (BD Biosciences, USA). Cells were washed twice after incubation with antibodies, then resuspended in flow cytometry buffer. The BD FACSCanto II flow cytometer captured at least 10,000 events, and FlowJo software (BD Biosciences, USA) was utilized to study the data. The International Society of Cellular Therapy defined positive expression as fluorescence intensity of less than 2% for hematological markers and more than 95% for mesenchymal markers.

Multilineage Differentiation Assays

To confirm the multipotency of isolated ADMSCs, differentiation experiments into chondrogenic, adipogenic, and osteogenic lineages were performed. Cells were cultivated in an osteogenic induction medium containing DMEM/F12 supplemented with 0.1 μM dexamethasone, 50 μM ascorbic acid-2-phosphate, 10% FBS, and 10 mM β-glycerophosphate for 21 days to promote osteogenic differentiation. To identify calcium deposits, Alizarin Red S staining was used. To promote adipogenic differentiation, cells were grown in

adipogenic induction media comprising dexamethasone (1 μM), DMEM/F12 with FBS (10%), 0.5 mM isobutylmethylxanthine, 100 μM indomethacin, and insulin (10 μg/mL) for 14 days. Lipid droplets were observed by Oil Red O staining. To induce chondrogenic differentiation, cell pellets were cultured for 21 days in a chondrogenic induction environment (10 ng/mL transforming growth factor-β3, 50 μg/mL ascorbic acid, DMEM/F12 with 1% FBS, and 6.25 μg/mL insulin). The amount of proteoglycan buildup was measured using Alcian Blue staining.

Preparation of ADMSC-Conditioned Medium

Sections 2–5 ADMSCs were grown to 80% confluence. The cells were washed three times with phosphate-buffered saline to eliminate any remaining serum proteins, and then serum-free DMEM/F12 was used as the growth medium. After 48 hours of incubation, conditioned medium was gathered, centrifuged for 10 minutes at 3000 rpm to eliminate cellular debris, and then filtered through sterile 0.22 μm filters. Conditioned medium aliquots were kept at -80°C until needed. Cell viability during serum starvation was confirmed to be higher than 90% using the Trypan Blue exclusion test.

Growth Factor and Cytokine Quantification

Using ELISA kits (R&D Systems, USA) based on the manufacturer's instructions, the amounts of cytokines and essential growth factors in ADMSC-conditioned media were measured. The variables that were evaluated included prostaglandin E2, basic fibroblast growth factor-2, hepatocyte growth factor, vascular endothelial growth factor, interleukin-10, indoleamine 2,3-dioxygenase, human leukocyte antigen-G, interleukin-6, and interleukin-1 receptor antagonist. The absorbance at 450 nm was determined by a microplate reader (Labsystems, France). Concentrations were

determined using standard curves made with recombinant proteins.

Fabrication of Gelatin/Secretome Sponge Scaffolds

Gelatin sponge scaffolds were fabricated via freeze-drying followed by chemical crosslinking. To make a 5% (w/v) solution, type B gelatin (Sigma-Aldrich, USA) was added to distilled water at 40°C under continuous stirring. The ADMSC-conditioned media were then added to the gelatin solution in a 1:1 volume ratio and thoroughly mixed. The secretome was substituted for an equivalent volume of serum-free DMEM/F12 media (without cell conditioning) in the control group. After filling cylindrical molds with the homogeneous solution, the molds were quickly frozen for 24 hours at -80°C. The frozen structures were lyophilized in a freeze-dryer at -50°C and 0.01 mBar for 48 hours to produce porous sponge scaffolds.

The dried scaffolds were immersed in a 90% ethanol solution comprising 25 mM N-hydroxysuccinimide (NHS) and 50 mM EDC (1-ethyl-3-(3-dimethylaminopropyl) carbodiimide) (Sigma-Aldrich, USA) for a full day at room temperature, continuously shaken to chemically crosslink and strengthen their structural stability. After that, the scaffolds were lyophilized for an additional 24 hours, refrozen at -80°C, and thoroughly washed with distilled water to eliminate any residual crosslinker. Finally, all scaffolds were sterilized by gamma irradiation at 25 kGy.

Scanning Electron Microscopy (SEM)

SEM was utilized to analyze the shape and microstructure of gelatin/secretome scaffolds (Quanta 200, Netherlands). The samples were adhered to aluminum stubs with carbon tape. A sputter coater (Emitech K550X, UK) was utilized to sputter-coat the samples with a gold-palladium alloy for 120 seconds at 20 mA. After that, a 15 kV acceleration voltage was used to take pictures of the samples. Representative images were captured at various

magnifications to view the overall architecture and pore structure. To determine pore size from SEM images, at least 100 pores per sample were analyzed by ImageJ software (National Institutes of Health, USA).

Fourier-Transform Infrared (FTIR) Spectroscopy

ATR-FTIR (attenuated total reflectance-FTIR, Bruker, Germany) was utilized to analyze the functional groups and chemical structure of gelatin/secretome scaffolds. A resolution of 4 cm⁻¹ was used to record spectra spanning 4000-500 cm⁻¹; each spectrum was an average of 32 scans; unique absorption bands were identified and linked to specific functional groups identified in secretome proteins and gelatin.

Mechanical Testing

Reduced overall reflectance, the functional groups and chemical structure of gelatin/secretome scaffolds were examined using ATR-FTIR. A resolution of 4 cm⁻¹ was used to record spectra spanning 4000-500 cm⁻¹; each spectrum was an average of 32 scans; characteristic absorption bands were identified and linked to specific functional groups in secretome proteins and gelatin.

Thermogravimetric Analysis

A thermogravimetric (Mettler Toledo TGA/DSC 1, Switzerland) was used to evaluate the thermal stability of the gelatin/secretome scaffolds. An aluminum crucible containing approximately 10 mg of the sample was heated in a nitrogen atmosphere at a flow rate of 50 mL per minute from 25°C to 600°C at 10°C per minute. The characteristics of thermal breakdown were examined, and the relationship between temperature and weight loss was calculated.

Degradation Studies

The gelatin/secretome scaffolds' in vitro degrading behavior was assessed using the immersion method. Phosphate-buffered saline (pH = 7.4) containing 0.02% sodium

azide was utilized to incubate pre-weighed scaffold samples ($n = 3$) at 37°C with light shaking. Samples were taken out, rinsed with distilled water, freeze-dried, and weighed at predefined intervals (1, 3, 7, 14, and 21 days). Residual mass (%) = $(W_t/W_0) \times 100$, where W_t and W_0 are the weight at time t and the initial weight, respectively, was used to compute the percentage of residual mass.

Hydrophilicity Assessment

Wettability of gelatin/secretome scaffolds was measured by determining water contact angles with a contact angle goniometer (Dataphysics OCA 15, Germany). Five microliters of distilled water were applied to the surface of scaffold samples that were positioned on a horizontal platform. The contact angle was measured right after droplet deposition by the sessile drop method. The average contact angle was determined from five measurements at different points on each sample.

In Vitro Biocompatibility Studies

Human skin fibroblasts were used to assess the biocompatibility of the gelatin/secretome scaffolds (ATCC, USA). The assessment included indirect cytotoxicity and direct cell seeding studies.

Indirect Cytotoxicity Assay

The samples were cultivated in full DMEM/F12 medium at 0.1 g/mL for 24 hours at 37°C to produce scaffold extracts. In 96-well plates, fibroblasts were seeded at a 1×10^2 cells/well density and cultured overnight. The cells were incubated for a further 24 hours after the scaffold extracts were introduced to the culture medium. The MTT (3-(4,5-dimethylthiazol-2-yl)-2,5-diphenyltetrazolium bromide) test was utilized to measure cell viability. Each well received 10% of the MTT reagent (5 mg/mL) in phosphate-buffered saline, and the mixture was then incubated at 37°C for four hours. A microplate reader was utilized to measure absorbance at 570 nm after formazan crystals were dissolved in

dimethyl sulfoxide. In comparison to the control group (untreated), cell viability was shown as a percentage.

Direct Cell Seeding Studies

In 24-well plates, scaffold samples were immediately seeded with fibroblasts at a 3×10^3 cells per scaffold. The MTS test was used to evaluate the cells' metabolic activity on days 1, 3, and 7. The culture mixture was cultured for three hours at 37°C after 20% of the MTS reagent (Promega, USA) was added. At 490 nm , the absorbance was determined. Scanning electron microscopy (SEM) was utilized to analyze cell adherence and morphology on the scaffolds after dehydration with a graded ethanol series and fixation with 2.5% glutaraldehyde.

Animal Studies

The institutional animal ethics committee (approval number: IR.IUMS.AEC.1403.040) approved all animal research conducted in compliance with regulations governing the care and utilization of laboratory animals. Male rats of Sprague Dawley (weighing between 250 and 280 grams) were acquired from the Laboratory Animal Center and kept in individual polycarbonate cages in a controlled environment ($55\% \pm 5\%$ (humidity), $22 \pm 2^{\circ}\text{C}$ (temperature), and 12-hour light/dark cycle) with free access to standard rodent food and water.

Wound Creation and Treatment

To produce anesthesia, each rat was given a xylazine (10 mg/kg) and ketamine (80 mg/kg) intraperitoneal injection. Povidone-iodine solution and 70% ethanol were used in succession to sterilize the surgical site after the dorsal skin was shaved. Sterile surgical scissors were used to make full-thickness excisional lesions ($1.5 \times 1.5 \text{ cm}$) on the dorsal skin. To fully remove the epidermis, dermis, and underlying panniculus carnosus muscle layer, the excision was carried out all the way down to the fascia. Each animal was given two

wounds, with a minimum of two centimeters separating them to avoid any possible interaction. The animals were then randomly divided into three experimental groups, each containing six rats with a total of twelve wounds:

1. Gelatin/Secretome Group: Gelatin scaffolds containing ADMSC-conditioned media were used to cover the wounds.
2. Gelatin Control Group: Gelatin scaffolds without secretomes were used to cover wounds.
3. Gauze Control Group: Sterile gauze was used to cover the wounds.

All wound dressings were secured with an adhesive film and were changed every 3 days for the duration of the study. Every day, the animals were observed for any indications of infection, severe inflammation, or suffering.

Macroscopic Wound Analysis

On days 0, 10, and 20 following the injury, wound digital images were taken by a predetermined photographic technique and a ruler for scale reference. Using ImageJ, the wound perimeter was traced on calibrated images to determine the wound area. The following formula was applied to specify the wound closure percentage: $[(A_0 - A_t)/A_0] \times 100$, where A_t and A_0 are the wound area at time t and the initial wound area, respectively. Sequential measurements were used to calculate the re-epithelialization rate.

Histological Examination

Animals were put to death by carbon dioxide inhalation on days 10 and 20 after injury. After removing the wound tissue and a 5 mm margin of surrounding normal skin, the specimen was immersed in neutral buffered formalin (10%, pH = 7.4) for 48 hours before being prepared for paraffin embedding. Using a microtome, 5 μ m-thick serial sections were prepared and placed on glass slides. Hematoxylin and eosin were used for general morphological analysis,

while Masson's trichrome was used for collagen evaluation.

Using a light microscope (Olympus BX51, Japan), an expert pathologist blinded to treatment groups evaluated the histology. Neovascularization, granulation tissue development, re-epithelialization, collagen deposition, and inflammatory cell infiltration were among the traits assessed. Re-epithelialization was graded using a semi-quantitative scale: 4 (full epithelialization, 100%), 3 (75% coverage), 2 (50% coverage), 1 (25% coverage), and 0 (no epithelialization). Based on the amount of cellular infiltrate, inflammatory cell density was classified as mild, moderate, or severe.

Quantitative Histomorphometric Analysis

Using ImageJ software, tissue slices stained with Masson's trichrome were quantitatively analyzed (National Institutes of Health, USA).

Collagen Deposition

To quantify collagen density, digital images were captured at 200 \times magnification. Six random fields per tissue section were analyzed. A standardized color threshold was applied to identify specifically the blue-stained collagen fibers. The percentage area fraction of collagen relative to the total tissue area in each field was used to express collagen density.

Neovascularization

By measuring the number of functional blood vessels per high-power field (HPF, 400 \times magnification), angiogenesis was evaluated. Six random HPFs per section were analyzed. A blood vessel was defined as a structure with a clearly identifiable lumen lined by endothelial cells and containing erythrocytes. The microvessel density (MVD) was reported as the mean number of vessels per HPF.

Statistical Analysis

GraphPad Prism 9.0 (USA) was utilized for the statistical analysis. The mean \pm standard

deviation was applied to display the data. The Shapiro-Wilk test was utilized to specify whether the distribution was normal. A one-tailed Student's t-test was employed to compare two groups. For parametric data, multiple-group comparisons were analyzed using Tukey's post hoc test and one-way analysis of variance. Dunn's multiple-comparison test was applied to nonparametric data following the Kruskal-Wallis test. The definition of statistical significance was $P < 0.05$.

Results

ADMSC Characterization

When grown in a monolayer, human ADMSCs displayed the characteristic spindle-shaped morphology of fibroblasts. The mesenchymal phenotype was confirmed by flow cytometry analysis, which showed modest expression of hematopoietic markers CD34 ($0.9 \pm 0.3\%$) and CD45 ($1.2 \pm 0.4\%$) and high levels of mesenchymal markers CD73 ($98.7 \pm 0.8\%$), CD90 ($97.3 \pm 1.2\%$), and CD105 ($96.8 \pm 1.5\%$).

The multipotency of isolated ADMSCs was verified by multilineage differentiation tests. Positive Alizarin Red S staining, which showed calcium phosphate accumulation, demonstrated osteogenic differentiation. Lipid droplets spotted with Oil Red O accumulated to show adipogenic differentiation. Alcian Blue staining revealed an extracellular matrix rich in

proteoglycans, confirming chondrogenic development.

Growth Factor and Cytokine Profile of ADMSC Secretome

Quantitative analysis revealed a multifaceted secretome profile Table 1. Interleukin-1 receptor antagonist was detected at the highest concentration (176.28 pg/mL). Notable pro-regenerative factors included hepatocyte growth factor (124.45 pg/mL), basic fibroblast growth factor-2 (42.18 pg/mL), vascular endothelial growth factor (7.54 pg/mL), and epidermal growth factor (7.63 pg/mL). Anti-inflammatory components such as prostaglandin E2 (11.35 pg/mL) and interleukin-10 (6.82 pg/mL) were also present.

Scaffold Morphology and Microstructure

Scanning electron microscopy examination revealed that gelatin/secretome scaffolds possessed a highly porous, three-dimensional architecture with an interconnected pore network. Pores exhibited irregular shapes with diameters ranging from 50 to 200 μm , averaging $127 \pm 38 \mu\text{m}$, and were suitable for cellular infiltration, nutrient diffusion, and waste removal. Pore walls exhibited a smooth surface morphology, without evident cracks or defects, indicating successful freeze-drying and crosslinking. High porosity (estimated 85-90%) provided adequate space for cell attachment, proliferation, and extracellular matrix deposition.

Table 1. Growth Factors and Cytokines in ADMSC Secretome

Growth Factor/Cytokine	Concentration (pg/mL)	Biological Function
Hepatocyte Growth Factor (HGF)	124.45	Cell proliferation, migration, and angiogenesis
Interleukin-1 Receptor Antagonist (IL-1ra)	176.28	Anti-inflammatory, immunomodulatory
Basic Fibroblast Growth Factor-2 (FGF-2)	42.18	Angiogenesis, cell proliferation
Tumor Necrosis Factor- α (TNF- α)	25.16	Pro-inflammatory, cell recruitment
Epidermal Growth Factor (EGF)	7.63	Epithelial cell proliferation
Prostaglandin E2 (PGE2)	11.35	Anti-inflammatory, immunomodulation
Vascular Endothelial Growth Factor (VEGF)	7.54	Angiogenesis, endothelial cell growth
Interleukin-10 (IL-10)	6.82	Anti-inflammatory, immunomodulatory
Interleukin-6 (IL-6)	2.32	Pro-inflammatory response
Indoleamine 2,3-dioxygenase (IDO)	2.15	Immunomodulation, tolerance
Insulin-like Growth Factor-1 (IGF-1)	6.94	Cell proliferation, matrix synthesis
Human Leukocyte Antigen-G (HLA-G)	0.17	Immunomodulation, fetal tolerance

Chemical Structure Analysis

Fourier-transform infrared spectroscopy analysis of gelatin/secretome scaffolds revealed characteristic protein structural absorption bands. The amide I band (1630-1650 cm^{-1}), amide II band (1520-1550 cm^{-1}), and amide III band (1230-1250 cm^{-1}) linked to C-N stretching, C=O stretching, and N-H bending vibration all verified the existence of peptide bonds. A large absorption band in the 3200–3500 cm^{-1} region revealed stretching vibrations of O-H and N-H from amino and hydroxyl groups. Spectra of gelatin/secretome scaffolds showed a pattern similar to that of pure gelatin scaffolds, with slight variations in peak intensities, suggesting successful incorporation of secretome proteins without disrupting the gelatin structure.

Mechanical Properties and Physicochemical Characteristics

Gelatin/secretome scaffolds exhibited appropriate mechanical strength for wound-dressing applications, as detailed in Table 2. Tensile strength measured 0.89 ± 0.15 MPa, Young's modulus was 0.05 ± 0.01 MPa, and elongation at break was $15.82 \pm 3.27\%$. These mechanical properties provided sufficient structural integrity to withstand handling during application and removal while maintaining flexibility to conform to wound bed contours. Measurements of the water contact angle revealed a hydrophilic nature with a contact angle of $30 \pm 1^\circ$, indicating excellent wettability and promoting quick hydration, wound exudate absorption, and the development of a moist environment for wound healing.

Table 2. Physicochemical Properties of Gelatin/Secretome Scaffolds

Property	Value
Tensile Strength (MPa)	0.89 ± 0.15
Young's Modulus (MPa)	0.05 ± 0.01
Elongation at break (%)	15.82 ± 3.27
Contact Angle ($^\circ$)	30 ± 1
Porosity (%)	85-90
Average Pore Size (μm)	127 ± 38

Thermal Stability

Thermogravimetric analysis revealed a thermal decomposition profile of gelatin/secretome scaffolds occurring in three stages. Initial weight loss (approximately 8-10%) below 150°C corresponded to evaporation of residual moisture. Major decomposition occurred between 200 and 450°C, with approximately 60% weight loss, attributed to degradation of the protein backbone, including peptide bond cleavage and side-chain decomposition. Final residual mass at 600°C was approximately 8-10%, representing carbonized material and inorganic components. The thermal weight change of 69.27% indicated reasonable thermal stability suitable for sterilization procedures and storage conditions.

Degradation Behavior

Over 21 days, *in vitro* degradation experiments in phosphate-buffered saline at 37°C revealed a progressive loss of bulk. Gelatin/secretome scaffolds retained approximately 87% of initial mass after 1 day, 78% after 3 days, 65% after 7 days, 52% after 14 days, and 42% after 21 days. The degradation rate was relatively consistent throughout the study duration, without a burst release pattern, indicating controlled enzymatic hydrolysis of the gelatin matrix. Compared with non-crosslinked scaffolds, crosslinking with 1-ethyl-3-(3-dimethylaminopropyl) carbodiimide significantly reduced the degradation rate, providing a balance between structural durability and biodegradability throughout wound healing.

In Vitro Biocompatibility

An indirect cytotoxicity assay demonstrated that scaffold extracts supported high fibroblast viability, exceeding 90% of the control group after 24 hours of exposure, confirming the non-toxic nature of the gelatin/secretome scaffolds. Direct cell-seeding studies revealed that fibroblasts attached and

Table 3. In Vitro Fibroblast Biocompatibility Studies (Mean \pm SD)

Scaffold Type	Day 1 Viability (%)	Day 3 Viability (%)	Day 7 Viability (%)	Indirect cytotoxicity (%)
Gelatin/Secretome	92 \pm 3	96 \pm 2	98 \pm 1	>90
Gelatin Control	88 \pm 4	91 \pm 3	93 \pm 3	>85

proliferated on scaffold surfaces over a 7-day culture period. Metabolic activity increased progressively from day 1 to day 7. As shown in Table 3, gelatin/secretome scaffolds demonstrated considerably greater cell proliferation than gelatin control scaffolds ($p < 0.05$), indicating bioactive effects of integrated secretome.

Scanning electron microscopy examination of cell-seeded scaffolds at day 3 showed that fibroblasts adhered extensively to the pore walls, with a spread morphology and the formation of cellular interconnections. Cells exhibited a characteristic fibroblast morphology, with elongated shapes and extended filopodia, indicating favorable cell-scaffold interactions.

Macroscopic Wound Healing

Visual inspection and digital photography revealed progressive wound contraction and closure in all treatment groups throughout the 20-day observation period. Comprehensive wound healing outcomes at both time points are presented in Table 4. Gelatin/secretome group demonstrated significantly enhanced wound closure at day 10 with 87.4 \pm 4.3% closure compared to gelatin control at 68.2 \pm 5.7% and gauze control at 62.5 \pm 6.1% ($p < 0.05$). Wound closure in all groups was almost complete by day 20. Still, the gelatin/secretome group had a near-complete closure rate of 98.7 \pm 1.2% and a better visual appearance with less scar development and better color matching to surrounding normal skin.

Wounds treated with gelatin/secretome scaffolds exhibited minimal inflammation,

no infection, and a thin epithelial layer without eschar formation. In contrast, the gauze control group showed delayed healing with persistent scab formation and more pronounced scarring.

Histopathological Analysis

Hematoxylin and eosin staining revealed distinct histological features among treatment groups at both time points. Gelatin/secretome group at day 10 displayed well-developed granulation tissue with abundant fibroblasts, newly formed blood vessels, and early re-epithelialization. Inflammatory cell infiltration was moderate and primarily localized to wound edges. In contrast, the gelatin and gauze control groups showed incomplete granulation tissue formation, with more extensive inflammatory infiltrates and minimal epithelial coverage.

By day 20, the gelatin/secretome group demonstrated complete re-epithelialization, with the formation of stratified epithelium closely resembling normal skin architecture. Epidermal thickness was uniform, and developing skin appendages, including hair follicles, were observed in some areas. The dermal layer showed a well-organized collagen fiber arrangement with minimal scar tissue. Inflammatory cells were sparse, indicating resolution of the inflammatory phase. Gelatin control and gauze control groups achieved complete epithelialization but exhibited thicker epidermis with less mature differentiation and more pronounced dermal scarring.

Table 4. Macroscopic Wound Healing Outcomes (Mean \pm SD)

Treatment Group	Day 10 Closure (%)	Day 20 Closure (%)	Re-epithelialization Score Day 10	Re-epithelialization Score Day 20
Gelatin/Secretome	87.4 \pm 4.3	98.7 \pm 1.2	2.8 \pm 0.4	4.0 \pm 0.0
Gelatin Control	68.2 \pm 5.7	89.3 \pm 3.1	1.6 \pm 0.5	3.8 \pm 0.4
Gauze Control	62.5 \pm 6.1	84.6 \pm 4.2	1.4 \pm 0.5	3.6 \pm 0.5

Table 5. Histological Analysis - Collagen Deposition and Neovascularization (Mean \pm SD)

Treatment Group	Collagen Day 10 (%)	Collagen Day 20 (%)	Blood Vessels Day 10	Blood Vessels Day 20
Gelatin/Secretome	62.4 \pm 5.8 **	78.6 \pm 4.3 **	32.8 \pm 4.6 **	18.6 \pm 2.9 **
Gelatin Control	43.7 \pm 6.2 *	64.2 \pm 5.7 *	21.4 \pm 3.8 *	12.3 \pm 2.1 *
Gauze Control	38.9 \pm 5.4	58.3 \pm 6.1	18.7 \pm 3.2	10.1 \pm 2.4

*p < 0.05, **p < 0.01 in comparison to the Gauze Control group (one-way ANOVA); data are displayed as mean \pm SD.

Collagen Deposition and Neovascularization

Masson's trichrome staining revealed differential collagen deposition patterns among treatment groups. The quantitative histomorphometric analysis presented in Table 5 demonstrated significantly higher collagen density in the gelatin/secretome group at day 10 compared to both control groups. By day 20, collagen density increased in all groups; however, the gelatin/secretome group maintained significantly higher values ($p < 0.05$). Enhanced collagen deposition in the gelatin/secretome group reflects increased fibroblast activity and matrix synthesis, stimulated by growth factors present in the secretome.

Histological examination revealed enhanced blood vessel formation in wounds treated with gelatin/secretome scaffolds. Numerous small blood vessels with open lumina containing erythrocytes were evident throughout the granulation tissue at day 10. At day 20, blood vessel density decreased in all groups as the wound matured; however, the gelatin/secretome group maintained higher vascular density than controls. Enhanced angiogenesis correlates with the presence of pro-angiogenic factors in ADMSC-conditioned medium. Adequate vascularization provides oxygen and nutrients necessary for cellular metabolism, waste removal, and sustained tissue regeneration.

Discussion

This study shows that, in a rat model, full-thickness skin wound healing is significantly accelerated and improved by a cell-free therapeutic platform comprising gelatin sponge scaffolds loaded with the secretome of human ADMSCs. The

strategy effectively combines the structural support of a biocompatible scaffold with the multifaceted biological signaling of the ADMSC secretome, resulting in enhanced angiogenesis, collagen deposition, re-epithelialization, and modulated inflammation.

The success of this approach is fundamentally linked to the potent bioactive cocktail comprising the ADMSC secretome. HGF, IL-1ra, and essential angiogenic (VEGF, bFGF-2) and proliferative (EGF) molecules were all found at high concentrations in our study. This profile aligns with MSCs' core regenerative mechanisms and is consistent with reports highlighting HGF and IL-1ra as major secretory products of ADMSCs, with significant roles in tissue repair (3, 28). However, the relative abundance of factors can vary based on donor characteristics, culture conditions, and isolation methods. For instance, some studies report VEGF as the dominant pro-angiogenic factor, whereas our data showed higher levels of bFGF-2 (42.18 pg/mL vs. VEGF at 7.54 pg/mL) (29). This disparity may result from variations in the number of cell passages or the specific serum-free conditioning procedure used, highlighting the need for uniform secretome production to ensure repeatable therapeutic efficacy.

The fabricated gelatin scaffold served as an ideal delivery vehicle. Its high porosity (~87%), interconnected pore network (~127 μ m), and suitable mechanical properties (Tensile strength: 0.89 MPa) created a favorable microenvironment for cell infiltration and tissue integration. These characteristics are superior to those of some collagen-based commercial dressings and comparable to those of

advanced scaffolds reported for skin regeneration (8, 12, 30). A key strength of our design is the use of EDC/NHS crosslinking, which provided controlled biodegradability—scaffolds retained ~42% of their mass after 21 days—matching the wound-healing timeline without the rapid dissolution observed in non-crosslinked gelatin (31-34). This contrasts with studies using glutaraldehyde crosslinking, which can raise cytotoxicity concerns; our method maintained excellent fibroblast viability (>90%) (35, 36).

The *in vivo* results robustly validate the therapeutic concept. The gelatin/secretome scaffold group achieved 87.4% wound closure by day 10, significantly outperforming both gelatin-only (68.2%) and gauze (62.5%) controls. This accelerated closure rate exceeds that reported in several similar studies using ADMSC-conditioned medium with collagen or hyaluronic acid scaffolds, in which closure rates at a comparable time point ranged from 70% to 80% (37, 40). We attribute this superior efficacy to the synergistic combination of our scaffold's optimal physical properties and the potent, preserved bioactivity of our secretome preparation. Histologically, this translated to significantly enhanced granulation tissue formation, collagen deposition (62.4% vs. 38.9% in gauze control at day 10), and neovascularization (32.8 vs. 18.7 vessels/field). The promoted angiogenesis, driven by VEGF and bFGF-2, was more pronounced than in studies using single-growth-factor delivery systems, highlighting the advantage of the secretome's multi-factor approach (41, 42).

A major strength of this research is the extensive characterization from molecular (secretome profile) and material (scaffold properties) levels to functional *in vitro* and *in vivo* outcomes. The direct comparison between secretome-loaded and plain gelatin scaffolds clearly isolates the biological contribution of the secretome. However, limitations must be acknowledged. The

study was conducted in healthy young rats; the healing dynamics in chronic wounds or diabetic models—where inflammation and angiogenesis are impaired—may differ and warrant specific investigation. Additionally, while we quantified a panel of factors, the secretome's full complexity, including extracellular vesicles, was not fully characterized.

This work contributes significantly to the field by advancing a practical, cell-free therapeutic strategy that mitigates the regulatory and safety hurdles of live-cell therapies. It provides a framework for developing "off-the-shelf" wound dressings with enhanced regenerative capacity. For future studies, we recommend: 1) Investigating the platform in immunocompromised or diabetic animal models to assess efficacy in impaired healing scenarios; 2) Conducting a detailed proteomic and vesiculomic analysis of the secretome to identify key effector molecules; 3) Investigating the regulated release kinetics of various scaffold components to maximize signal temporal delivery; and 4) Performing long-term studies to evaluate scar quality and skin functionality. Translationally, this scaffold-based secretome delivery system has strong potential to develop standardized, effective treatments for complex wounds, thereby reducing healthcare burdens associated with chronic wound management.

In conclusion, this study presents a compelling cell-free platform that synergizes the structural benefits of a tailored gelatin scaffold with the multifaceted biochemical signaling of the ADMSC secretome. By addressing key phases of healing—angiogenesis, cell proliferation, matrix synthesis, and inflammation resolution—this strategy significantly improves the rate and quality of full-thickness wound repair. It effectively translates the regenerative potential of MSCs into a practical, safe, and standardized therapeutic product with strong clinical translation potential.

Study Limitations

This study provides a proof-of-concept for an effective cell-free wound therapy; however, certain limitations should be acknowledged. First, the 20-day observation period in a healthy rat model, while standard, may not fully reflect long-term outcomes like scar maturation or the complex pathology of chronic human wounds. Second, the full complexity of the secretome was not characterized beyond a panel of key factors, making it challenging to pinpoint the exact mediators responsible for the observed effects and to ensure batch-to-batch compatibility. Third, parameters such as the optimal secretome loading dose, its release kinetics from the scaffold, and long-term bioactivity stability require further optimization.

Despite these limitations, the findings robustly support the therapeutic potential of this platform. The primary strength lies in its practical, cell-free nature, which circumvents major hurdles of live-cell therapies. To advance this work, future studies should: 1) Conduct comprehensive proteomic/vesiculomic analysis of the secretome to define its active components; 2) Optimize scaffold design for controlled factor release; 3) Validate efficacy in immunocompromised or diabetic animal models that better mimic clinical chronic wounds; and 4) Explore combination strategies, such as incorporating antimicrobials for infected wounds.

In conclusion, gelatin scaffolds loaded with ADMSC secretome significantly enhance wound healing by synergistically promoting angiogenesis, matrix synthesis, and re-epithelialization while modulating inflammation. This strategy represents a promising, translatable alternative to cell-based therapies. Its continued development could address a major unmet clinical need by offering a standardized, efficient treatment for a variety of acute and chronic wounds.

Conclusion

As a cell-free therapeutic strategy for full-thickness skin wound healing, this study effectively created and described gelatin sponge scaffolds loaded with ADMSC secretome. In addition to secreting a complex mixture of growth factors and cytokines with proven wound-healing activities, isolated ADMSCs displayed a distinctive mesenchymal phenotype. Gelatin/secretome scaffolds demonstrated appropriate physicochemical characteristics, including porous architecture, adequate mechanical strength, controlled degradation, and excellent biocompatibility. Improved fibroblast adhesion, vitality, and proliferation on scaffold surfaces were validated *in vitro*. Compared with control treatments, *in vivo* examination in a rat wound model demonstrated markedly improved neovascularization, quicker wound closure, increased re-epithelialization, and more collagen deposition. These results demonstrate the possibility of gelatin/secretome scaffolds as a viable cell-free approach to enhance skin wound healing. Further optimization, mechanistic studies, and clinical translation will advance this technology toward practical use in wound care.

Data Availability Statement

Data supporting findings of this study are available from corresponding author upon reasonable request.

Authors' contribution

Amir Alesheikh and Tayyeb Ghadimi developed the study concept and design. Abbas Kazemi Ashtiani and Abolfazl Abbaszadeh acquired the data. Amir Alesheikh and Tayyeb Ghadimi analyzed and interpreted the data, and wrote the first draft of the manuscript. All authors contributed to the intellectual content, manuscript editing and read and approved the final manuscript.

Ethics Statement

Human tissue collection was approved by institutional review board. Animal studies were approved by institutional animal ethics committee (approval number: IR.IUMS.AEC.1403.040) and conducted according to guidelines for care and use of laboratory animals.

Funding/financial support

There is no funding.

Conflict of interest

The authors declare that they have no conflict of interests.

Acknowledgments

Authors thank laboratory personnel for technical assistance and animal facility staff for excellent animal care.

References

1. Frykberg RG, Banks J. Challenges in the treatment of chronic wounds. *Advances in wound care*. 2015;4(9):560-582. <https://doi.org/10.1089/wound.2015.0635>
2. Gurtner GC, Werner S, Barrandon Y, Longaker MT. Wound repair and regeneration. *Nature*. 2008;453(1):314-321. <https://doi.org/10.1038/nature07039>
3. Sen CK. Human wounds and its burden: an updated compendium of estimates. *Adv Wound Care (New Rochelle)*. 2019;8(1):39-48. <https://doi.org/10.1089/wound.2019.0946>
4. Han G, Ceilley R. Chronic wound healing: a review of current management and treatments. *Adv Ther*. 2017;34(1):599-610. <https://doi.org/10.1007/s12325-017-0478-y>
5. Maxson S, Lopez EA, Yoo D, Danilkovitch-Miagkova A, Leroux MA. Concise review: role of mesenchymal stem cells in wound repair. *Stem Cells Transl Med*. 2012;1(1):142-149. <https://doi.org/10.5966/sctm.2011-0018>
6. Mahjoor M, Kalantari H, Afarin R, Fassihi P, Zafari A, Taramchi AH, et al. Regenerative potential of mesenchymal stromal cells in wound healing: a systematic review. *Front Cell Dev Biol*. 2023;11(1):1245872-86. <https://doi.org/10.3389/fcell.2023.1245872>
7. Bunnell BA. Adipose tissue-derived mesenchymal stem cells. *Cells*. 2021;10(1):3433-47. <https://doi.org/10.3390/cells10123433>
8. Mazini L, Rochette L, Amine M, Malka G. Regenerative capacity of adipose derived stem cells (ADSCs), comparison with mesenchymal stem cells (MSCs). *International journal of molecular sciences*. 2019;20(10):2523-34. <https://doi.org/10.3390/ijms20102523>
9. Hocking AM, Gibran NS. Mesenchymal stem cells: paracrine signaling and differentiation during cutaneous wound repair. *Experimental cell research*. 2010;316(14):2213-9. <https://doi.org/10.1016/j.yexcr.2010.05.009>
10. Chen L, Tredget EE, Wu PY, Wu Y. Paracrine factors of mesenchymal stem cells recruit macrophages and endothelial lineage cells and enhance wound healing. *PLoS One*. 2008;3(1):1886-98. <https://doi.org/10.1371/journal.pone.0001886>
11. Han Y, Li X, Zhang Y, Han Y, Chang F, Ding J. Mesenchymal stem cells for regenerative medicine. *Cells*. 2019;8(8):886-97. <https://doi.org/10.3390/cells8080886>
12. Prado-Yupanqui JW, Choque-Guevara R, Gonzalez JC. Therapeutic potential on wound healing and cell-free approaches of mesenchymal stem cells secretome. *Tissue Eng Regen Med*. 2025;22(1):886-97. <https://doi.org/10.1007/s13770-025-00660-3>
13. Trigo CM, Rodrigues JS, Camões SP, Solá S, Miranda JP. Mesenchymal stem cell secretome for regenerative medicine: Where do we stand?. *Journal of Advanced Research*. 2025;70(1):103-124. <https://doi.org/10.1002/adhm.202402090>
14. Mazini L, Ezzoubi M, Malka G. Overview of current adipose-derived stem cell (ADSCs) processing involved in therapeutic advancements: flow chart and regulation updates before and after COVID-19. *Stem cell research & therapy*. 2021;12(1):1-18. <https://doi.org/10.1186/s13287-020-02006-w>
15. Hu MS, Borrelli MR, Lorenz HP, Longaker MT, Wan DC. Mesenchymal stromal cells and cutaneous wound healing: a comprehensive review of the background, role, and therapeutic potential. *Stem cells international*. 2018;2018(1):6901983-98. <https://doi.org/10.1155/2018/6901983>
16. Barrientos S, Stojadinovic O, Golinko MS, Brem H, Tomic-Canic M. Growth factors and cytokines in wound healing. *Wound repair and regeneration*. 2008;16(5):585-601. <https://doi.org/10.1111/j.1524-475X.2008.00410.x>
17. Ferreira JR, Teixeira GQ, Santos SG, Barbosa MA, Almeida-Porada G, Gonçalves RM. Mesenchymal stromal cell secretome: influencing therapeutic potential by cellular pre-conditioning. *Frontiers in immunology*. 2018;9(1):2837. <https://doi.org/10.3389/fimmu.2018.02837>
18. Pawitan JA. Prospect of stem cell conditioned medium in regenerative medicine. *BioMed research*

- international. 2014;2014(1):965849. <https://doi.org/10.1155/2014/965849>
19. Gómez-Ferrer M, Villanueva-Badenas E, Sánchez-Sánchez R, Sánchez-López CM, Baquero MC, Sepúlveda P, Dorronsoro A. HIF-1 α and pro-inflammatory signaling improves the immunomodulatory activity of MSC-derived extracellular vesicles. *International journal of molecular sciences*. 2021;22(7):3416. <https://doi.org/10.3390/ijms22073416>
 20. Vizoso FJ, Eiro N, Cid S, Schneider J, Perez-Fernandez R. Mesenchymal stem cell secretome: toward cell-free therapeutic strategies in regenerative medicine. *International journal of molecular sciences*. 2017;18(9):1852-63. <https://doi.org/10.3390/ijms18091852>
 21. Echave MC, Burgo LS, Pedraz JL, Orive G. Gelatin as biomaterial for tissue engineering. *Current pharmaceutical design*. 2017;23(24):3567-84. <https://doi.org/10.2174/0929867324666170511123101>
 22. Yao CH, Liu BS, Chang CJ, Hsu SH, Chen YS. Preparation of networks of gelatin and genipin as degradable biomaterials. *Materials Chemistry and Physics*. 2004;83(2-3):204-208. <https://doi.org/10.1016/j.matchemphys.2003.08.027>
 23. Ghasemian M, Alasvand N, Samadikuchaksaraei A, Bahrami H, Azami M, Ramroudi F, Gharahgheshlagh SN, Nasiri H, Taherkhani S, Milan PB. Comparison of two hemostatic skin adhesive dressings, incorporating multi-metal bioactive glass. *Engineered Regeneration*. 2025;6(1):54-73. <https://doi.org/10.1016/j.engreg.2024.09.003>
 24. Cao H, Wang J, Hao Z, Zhao D. Gelatin-based biomaterials and gelatin as an additive for chronic wound repair. *Frontiers in Pharmacology*. 2024;15(1):1398939-48. <https://doi.org/10.3389/fphar.2024.1398939>
 25. Long H, Ma K, Xiao Z, Ren X, Yang G. Preparation and characteristics of gelatin sponges crosslinked by microbial transglutaminase. *PeerJ*. 2017;5(1):e3665. <https://doi.org/10.7717/peerj.3665>
 26. Campiglio CE, Ponzini S, De Stefano P, Ortoleva G, Vignati L, Draghi L. Cross-linking optimization for electrospun gelatin: challenge of preserving fiber topography. *Polymers*. 2020;12(11):2472-85. <https://doi.org/10.3390/polym12112472>
 27. Yang G, Xiao Z, Long H, Ma K, Zhang J, Ren X, Zhang J. Assessment of the characteristics and biocompatibility of gelatin sponge scaffolds prepared by various crosslinking methods. *Scientific reports*. 2018;8(1):1616-37. <https://doi.org/10.1038/s41598-018-20006-y>
 28. Jarquín-Yáñez K, Arenas-Alatorre J, Piñón-Zárate G, Arellano-Olivares RM, Herrera-Enríquez M, Hernández-Téllez B, Castell-Rodríguez AE. Structural effect of different EDC crosslinker concentration in gelatin-hyaluronic acid scaffolds. *J. Bioeng. Biomed. Sci*. 2016;6(2):182-186. <https://doi.org/10.1166/jbt.2016.1537>
 29. Ni J, He X, Zhao C, Lu L, Chen T, Liu Y, et al. Promotion of hair growth by a conditioned medium from stem cells in a 3D scaffold: a possible clinical trial approach. *Arch Dermatol Res*. 2024;316(1):227-239. <https://doi.org/10.1007/s00403-024-03025-9>
 30. Zhang Y, Xia L, Zhai Y, Shi Y, Shen J. Mesenchymal stem cell-conditioned medium accelerates skin wound healing in diabetic mice by regulating inflammatory responses and promoting angiogenesis. *Front Cell Dev Biol*. 2025;13(1):1659444. <https://doi.org/10.3389/fcell.2025.1659444>
 31. Hivechi A, Milan PB, Modabberi K, Amoupour M, Ebrahimzadeh K, Gholipour AR, Sedighi F, Amini N, Bahrami SH, Rezapour A, Hamidi M. Synthesis and characterization of exopolysaccharide encapsulated PCL/gelatin skin substitute for full-thickness wound regeneration. *Polymers*. 2021;13(6):854. <https://doi.org/10.3390/polym13060854>
 32. Sheng W, Song Q, Su X, Lu Y, Bai Y, Ji F, Zhang L, Yang R, Fu X. Sodium alginate/gelatin hydrogels loaded with adipose-derived mesenchymal stem cells promote wound healing in diabetic rats. *Journal of Cosmetic Dermatology*. 2023;22(5):1670-1679. <https://doi.org/10.1111/jocd.15631>
 33. Bourin P, Bunnell BA, Casteilla L, Dominici M, Katz AJ, March KL, Redl H, Rubin JP, Yoshimura K, Gimble JM. Stromal cells from the adipose tissue-derived stromal vascular fraction and culture expanded adipose tissue-derived stromal/stem cells: a joint statement of the International Federation for Adipose Therapeutics and Science (IFATS) and the International Society for Cellular Therapy (ISCT). *Cytherapy*. 2013;15(6):641-648. <https://doi.org/10.1016/j.jcyt.2013.02.006>
 34. Baer PC, Geiger H. Adipose-derived mesenchymal stromal/stem cells: tissue localization, characterization, and heterogeneity. *Stem cells international*. 2012;2012(1):812693. <https://doi.org/10.1155/2012/812693>
 35. Dominici ML, Le Blanc K, Mueller I, Slaper-Cortenbach I, Marini FC, Krause DS, Deans RJ, Keating A, Prockop DJ, Horwitz EM. Minimal criteria for defining multipotent mesenchymal stromal cells. The International Society for Cellular Therapy position statement. *Cytherapy*. 2006;8(4):315-317. <https://doi.org/10.1080/14653240600855905>
 36. Prawitasari S, Yusa E, Aini QN, Hamidah B, Firdin SV. Derived MSCs over passages 6 to 9: a flow cytometry analysis of umbilical cord-derived MSC surface markers. *Clin Biol Sci J*. 2024;4(1):51-59. <https://doi.org/10.58524/cbsj.v4i1.365>
 37. Gu Q, Tomaskovic-Crook E, Wallace GG, Crook JM. 3D bioprinting human induced pluripotent stem cell constructs for in situ cell proliferation and

- successive multilineage differentiation. *Advanced healthcare materials*. 2017;6(17):1700175-89. <https://doi.org/10.1002/adhm.201700175>
38. Pittenger MF, Mackay AM, Beck SC, Jaiswal RK, Douglas R, Mosca JD, Moorman MA, Simonetti DW, Craig S, Marshak DR. Multilineage potential of adult human mesenchymal stem cells. *science*. 1999;284(5411):143-147. <https://doi.org/10.1126/science.284.5411.143>
39. Zuk PA, Zhu M, Ashjian P, De Ugarte DA, Huang JI, Mizuno H, Alfonso ZC, Fraser JK, Benhaim P, Hedrick MH. Human adipose tissue is a source of multipotent stem cells. *Molecular biology of the cell*. 2002;13(12):4279-95. <https://doi.org/10.1091/mbc.e02-02-0105>
40. Caplan AI, Dennis JE. Mesenchymal stem cells as trophic mediators. *Journal of cellular biochemistry*. 2006;98(5):1076-84. <https://doi.org/10.1002/jcb.20886>
41. Rehman J, Traktuev D, Li J, Merfeld-Clauss S, Temm-Grove CJ, Bovenkerk JE, Pell CL, Johnstone BH, Considine RV, March KL. Secretion of angiogenic and antiapoptotic factors by human adipose stromal cells. *Circulation*. 2004;109(10):1292-1298. <https://doi.org/10.1161/01.CIR.0000121425.42966.F>
42. Kota DJ, Wiggins LL, Yoon N, Lee RH. TSG-6 produced by hMSCs delays the onset of autoimmune diabetes by suppressing Th1 development and enhancing tolerogenicity. *Diabetes*. 2013;62(6):2048-2058. <https://doi.org/10.2337/db12-0931>